Biogeosciences

Open Access

Processes of ammonia air–surface exchange in a fertilized *Zea mays* canopy

J. T. Walker[1]**, M. R. Jones**[1,5]**, J. O. Bash**[2]**, L. Myles**[3]**, T. Meyers**[3]**, D. Schwede**[2]**, J. Herrick**[4]**, E. Nemitz**[5]**, and W. Robarge**[6]

[1]National Risk Management Research Laboratory, US Environmental Protection Agency, Office of Research and Development, Durham, NC 27711, USA
[2]National Exposure Research Laboratory, US Environmental Protection Agency, Office of Research and Development, Durham, NC 27711, USA
[3]National Oceanic and Atmospheric Administration, Air Resources Laboratory, Oak Ridge, TN 37831, USA
[4]National Center for Environmental Assessment, US Environmental Protection Agency, Office of Research and Development, Durham, NC 27711, USA
[5]Centre for Ecology and Hydrology (CEH), Edinburgh, Bush Estate, Penicuik, EH26 0QB, UK
[6]Department of Soil Science, North Carolina State University, Raleigh, NC 27695, USA

Correspondence to: J. T. Walker (walker.johnt@epa.gov)

Abstract. Recent incorporation of coupled soil biogeochemical and bi-directional NH_3 air–surface exchange algorithms into regional air quality models holds promise for further reducing uncertainty in estimates of NH_3 emissions from fertilized soils. While this represents a significant advancement over previous approaches, the evaluation and improvement of such modeling systems for fertilized crops requires process-level field measurements over extended periods of time that capture the range of soil, vegetation, and atmospheric conditions that drive short-term (i.e., post-fertilization) and total growing season NH_3 fluxes. This study examines the processes of NH_3 air–surface exchange in a fertilized corn (*Zea mays*) canopy over the majority of a growing season to characterize soil emissions after fertilization and investigate soil–canopy interactions. Micrometeorological flux measurements above the canopy, measurements of soil, leaf apoplast and dew/guttation chemistry, and a combination of in-canopy measurements, inverse source/sink, and resistance modeling were employed. Over a period of approximately 10 weeks following fertilization, daily mean and median net canopy-scale fluxes yielded cumulative total N losses of 8.4 % and 6.1 %, respectively, of the $134 \, kg \, N \, ha^{-1}$ surface applied to the soil as urea ammonium nitrate (UAN). During the first month after fertilization, daily mean emission fluxes were positively correlated with soil temperature and soil volumetric water. Diurnally, maximum hourly average fluxes of $\approx 700 \, ng \, N \, m^{-2} \, s^{-1}$ occurred near mid-day, coincident with the daily maximum in friction velocity. Net emission was still observed 5 to 10 weeks after fertilization, although mid-day peak fluxes had declined to $\approx 125 \, ng \, N \, m^{-2} \, s^{-1}$. A key finding of the surface chemistry measurements was the observation of high pH (7.0–8.5) in leaf dew/guttation, which reduced the ability of the canopy to recapture soil emissions during wet periods. In-canopy measurements near peak leaf area index (LAI) indicated that the concentration of NH_3 just above the soil surface was highly positively correlated with soil volumetric water, which likely reflects the influence of soil moisture on resistance to gaseous diffusion through the soil profile and hydrolysis of remaining urea. Inverse source/sink and resistance modeling indicated that the canopy recaptured $\approx 76 \%$ of soil emissions near peak LAI. Stomatal uptake may account for 12–34 % of total uptake by foliage during the day compared to 66–88 % deposited to the cuticle. Future process-level NH_3 studies in fertilized cropping systems should focus on the temporal dynamics of net emission to the atmosphere from fertilization to peak LAI and improvement of soil and cuticular resistance parameterizations.

1 Introduction

Livestock and crop production are responsible for 80 % of ammonia (NH_3) emissions in the US (US EPA, 2005). Fertilized soils account for 35 % (US EPA, 2005) of this fraction of total emissions. Fertilizer emissions vary temporally throughout the year in the US, reaching a maximum in the spring and a minimum in winter (Geobes et al., 2003). Approximately 60 % of emissions occur between March and June (Geobes et al., 2003). Temporal variability of NH_3 emissions influences the variability of ammonium (NH_4^+), sulphate (SO_4^{2-}), and nitrate (NO_3^-) aerosol formation in the atmosphere and wet and dry deposition of NH_x ($NH_x = NH_{3(g)} + NH_{4(s, aq)}^+$). Inorganic (i.e., NH_4^+-based) aerosol contributes significantly to total particulate matter with an aerodynamic diameter of $< 2.5 \, \mu m$ ($PM_{2.5}$) (Edgerton et al., 2005; Malm et al., 1994; Chow et al., 2006). As a component of atmospheric nitrogen deposition, NH_x contributes to soil acidification and aquatic and terrestrial eutrophication in sensitive ecosystems (Nihlgard, 1985; Paerl and Whitall, 1999).

Over the past decade, efforts have been made to incorporate the temporal variability of fertilizer emissions into inventories used for air quality modeling and assessments (Geobes et al., 2003; Gilliland et al., 2003). With respect to regional atmospheric models, emissions from fertilized soil have previously been processed and input separately from the physical and chemical components of the model that simulate transport, atmospheric transformations, and loss processes (Mathur and Dennis, 2003; Dennis et al., 2010). More recently, implementation of a bi-directional framework for NH_3 air–surface exchange in the Community Multi-scale Air Quality Model (CMAQ) (Bash et al., 2012) provides a basis for simulating fertilizer emissions in a process-oriented mode by incorporating the Environmental Policy Integrated Climate (EPIC) crop model, which includes soil biogeochemistry (Cooter et al., 2010).

Calculation of soil emissions within the bi-directional flux framework implemented in CMAQ increases the temporal resolution of emissions and simulates the net soil–canopy–atmosphere exchange in a mechanistically representative manner. Representation of the air–surface exchange process in a resistance-based two-layer compensation point framework (Nemitz et al., 2001; Cooter et al., 2010) accounts for the competing processes of emission from the soil and uptake or emission by the leaf cuticle and stomata, which collectively produce the net exchange of NH_3 with the atmosphere. Accurate simulation of the complexities introduced by the bi-directional nature of NH_3 fluxes is particularly important for agricultural systems in which the overlying canopy may recapture a significant fraction of soil emissions, thereby regulating the net canopy-scale flux (Harper et al., 2000; Nemitz et al., 2000; Denmead et al., 2008; Bash et al., 2010). While this modeling approach represents a clear improvement over the temporally allocated fertilizer inventory approach previously used, testing and improvement of both the bi-directional flux and soil biogeochemical models requires process-level field measurements over extended periods of time that capture the range of soil, vegetation, and atmospheric conditions that drive short-term (i.e., post-fertilization) and total growing season NH_3 fluxes within fertilized cropping systems. Further improvement of the biogeochemical model will require measurements for fertilizers currently in use and for those that will experience increased application in the future. For example, the use of nitrogen solutions mixed with urease inhibiting agents, which act to reduce NH_3 emissions, is likely to expand.

The purpose of this study was to examine the processes of NH_3 air–surface exchange in a fertilized corn (*Zea mays*) canopy over the majority of the growing season to characterize the dynamics of the emission process post-fertilization and investigate soil–canopy interactions once the canopy had reached peak leaf area. Here we describe the temporal variability of the net canopy-scale NH_3 fluxes, the quality of the flux and air concentration measurements, and the soil and vegetation chemistry underpinning the fluxes. We then focus on an intensive period of measurements within and above the canopy at peak leaf area to characterize soil/canopy interactions.

2 Methods

2.1 Site description

The measurement site was a flat, 200 ha agricultural field near Lillington, North Carolina, USA ($35°22'35.7''$ lat., $-78°46'45.1''$ long., 45 m elev.). Soils were primarily fine sandy loam (Exum series) with a texture of 21 %, 68 %, and 11 % sand, silt, and clay, respectively, and a bulk density of $1.42 \, g \, cm^{-3}$ over 0–10 cm depth. The entire field was planted in corn (*Zea mays*, Pioneer varieties 31G66 and 31P41, density of $\approx 70\,000$ plants ha^{-1}) and fertilized with $20 \, kg \, N \, ha^{-1}$ ammonium polyphosphate (injected) over a period of 6 days from 18 April 2007 (DOY 108) to 23 April 2007 (DOY 113), starting at the northern perimeter of the field and ending at the southern perimeter. The field was fertilized again over the course of 5 days from 25 May 2007 (DOY 145) to 29 May 2007 (DOY 149), again from the north to south, with $134 \, kg \, N \, ha^{-1}$ surface applied urea ammonium nitrate solution (UAN) containing a urease inhibitor (Agrotain®). Fertilizer was drip applied ("side-dressed") to the soil surface adjacent to the plants. The canopy reached a peak leaf area index (LAI, single-sided) of $2.9 \pm 0.6 \, m^2 \, m^{-2}$ and a maximum canopy height (h_c) of 2.2 m near 15 July 2007 (DOY 196) and had fully senesced by 21 August 2007 (DOY 233). Measurements presented in this paper cover the period 22 May 2007 (DOY 142) to 2 August 2007 (DOY 214).

2.2 Ammonia concentrations and fluxes

Above-canopy NH_3 fluxes were calculated using the modified Bowen ratio (MBR) method (Meyers et al., 1996). The MBR method assumes that the turbulent diffusivity of NH_3 is similar to the turbulent diffusivity of heat such that

$$F_{NH_3} = \overline{w'T'}\frac{\Delta\overline{C}}{\Delta\overline{T}} = \overline{w'T'}\frac{\overline{C}(z_1) - \overline{C}(z_2)}{\overline{T}(z_1) - \overline{T}(z_2)}, \qquad (1)$$

where F_{NH_3} is the air–canopy flux of NH_3, $\overline{w'T'}$ is the kinematic heat flux, and $\Delta\overline{C}$ and $\Delta\overline{T}$ are co-located mean NH_3 concentration and air temperature differences between heights z_1 and z_2 above the canopy. The ratio of the heat flux to the temperature gradient is also known as the eddy diffusivity for heat. The vertical NH_3 gradient was measured with a continuous flow "AMANDA" (Ammonia Measurement by ANnular Denuder sampling with online Analysis; Wyers et al., 1993) wet denuder system. Gaseous NH_3 was collected from the sample airstream ($30\,L\,min^{-1}$) in a wetted continuous-flow annular denuder using a stripping solution of $3.6\,mM$ $NaHSO_4$. The aqueous NH_3 concentration was determined by an online detector based on a selective ion membrane and conductivity analysis (detection limit $\approx 0.02\,\mu g\,NH_3\,m^{-3}$) by sequentially sampling each denuder. In theory, this approach does not suffer from aerosol interference and because the denuders are located at the atmospheric sampling point and employ a short ($30\,cm$ (L) by $2.54\,cm$ (O.D.)) Teflon inlet, sampling artifacts related to inlet surface losses are minimized. Fluxes were calculated using 30-min averaged concentrations measured between the lower and upper inlets, which increased in height from 0.3 to 2.5 m and 2.2 to 4.4 m, respectively, during the course of the experiment. The instrument was calibrated approximately bi-weekly using liquid NH_4^+ standards of 0, 50 and 500 ppb (RICCA, Arlington, TX, USA), and systematic offsets between denuders were corrected by periodic collocation of the denuder sampling boxes. An R. M. Young (Model 81000V, Traverse City, MI, USA) sonic anemometer was positioned at $z = 3.5\,m$ to measure wind speed and direction, kinematic heat flux, and momentum flux. Processing of 10 Hz sonic data included spike removal, 30-min detrending and 2-D coordinate rotation prior to calculation of 30-min averages. Data from the additional sonic anemometers referenced below were processed in the same manner. Air temperature was measured adjacent to each AMANDA sample inlet using fine wire copper-constantan thermocouples (OMEGA Engineering, Inc., Stamford, CT, USA). Fluxes and temperature profiles were reported as 30-min averages. The AMANDA Bowen ratio system was operational from DOY 142 to DOY 214 and is treated as the primary flux dataset in this analysis.

A second Bowen ratio system, operated for a shorter period of time (DOY 193–201), consisted of independent temperature and NH_3 gradients measured from a tower approximately 10 m west of the AMANDA tower. Ammonia concentration gradients were measured with duplicate dry annular denuders (URG Corp., Chapel Hill, NC, USA) at $z = 1.7\,m$ and 10 m. Two-hour samples were collected four times each day beginning at approximately 08:00, 10:00, 12:00, and 14:00 EDT. Glass impactors with cut-points of $2.5\,\mu m$ aerodynamic diameter were used to remove particles from the air sample stream. Mass-flow controllers (Aalborg, Orangeburg, NY, USA) maintained sample flow rates at $20\,L\,min^{-1}$. Methods for annular denuder preparation and extraction were based on US EPA Compendium Method IO 4.2 (US EPA, 1997). Annular denuders were coated with a 1% phosphorous acid solution and extracted with $\sim 10\,mL$ of $18\,M\Omega$ deionized water. Denuder extracts were analyzed by ion chromatography (Metrohm, Riverview, FL, USA) with a lower detection limit of $0.1\,mg\,L^{-1}$. Platinum resistance thermometers (Thermometrics Corp., Northridge, CA, USA) in aspirated radiation shields (Met One, Grants Pass, OR, USA) measured air temperature adjacent to denuder inlets at 0.1 Hz. A sonic anemometer (Model 81000V, R. M. Young) was placed at the upper height (10 m) to measure kinematic heat fluxes from 10 Hz wind speed and temperature data. Fluxes and temperature profiles were reported as 30-min averages.

In addition to above-canopy fluxes, an experiment was conducted in July, targeting peak leaf area, to examine in-canopy source/sink characteristics (Bash et al., 2010). In-canopy NH_3 concentrations were measured using duplicate phosphorous acid coated annular denuders (URG Corp.) mounted at 0.1, 0.3, 0.95, 1.5, and 2.25 m a.g.l., which were sampled for approximately 2 h each at an air flow rate of $20\,L\,min^{-1}$. Canopy height at the location of the profile measurements increased from 2.0 to 2.2 m during the in-canopy experiment. Denuder preparation and extraction also followed US EPA Compendium Method IO 4.2 (US EPA, 1997). After sampling, denuders were extracted with 2.5 mL deionized water and analyzed for NH_4^+ by ion chromatography (model DX120, Dionex Corporation, Sunnyvale, CA, USA). An ATI 3-D sonic anemometer (model SATI-3V, Applied Technologies, Inc., Longmont, CO, USA) was mounted on a height-adjustable bracket to measure wind speed and momentum fluxes within the canopy, and an R. M. Young sonic anemometer (Model 81000V) was located just above the top of the canopy. Soil and foliage fluxes were estimated from NH_3 concentration and turbulence profiles using an analytical first-order closure model (Bash et al., 2010).

Finally, 12-h integrated NH_3 concentrations were measured by annular denuder (URG Corp.) from DOY 142 to DOY 214 from on top of the mobile laboratory (4 m above the ground), which was approximately 30 m east of the AMANDA Bowen ratio system. Denuder protocols followed those of the in-canopy measurements, with the exception that air was sampled at a flow rate of $10\,L\,min^{-1}$ through a Teflon-coated cyclone (URG Corp.) with an aerodynamic cut-point of $2.5\,\mu m$.

2.3 Foliage, leaf water and soil measurements

Single-sided leaf area index (LAI) was measured approximately bi-weekly by destructive (prior to canopy closure) and optical methods (LICOR Model LAI-2000, LICOR Biosciences, Lincoln, NE, USA) along with plant height. Stomatal resistance was measured by leaf cuvette on three occasions corresponding to LAI values of 0.25, 1.0, and 2.9 (peak) $m^2 m^{-2}$ (LICOR Model LI6400 photosynthesis system). Measurements were taken on shaded and sunlit leaves over a range of photosynthetically active radiation (300–1800 $\mu mol\, m^{-2}\, s^{-1}$). Canopy wetness was quantified by leaf wetness sensors (Campbell Scientific Model 237 wetness sensing grid) positioned below and at the midpoint of the canopy, which provided 30-min data. On three occasions after canopy closure, leaf wetness (g $H_2O\, m^{-2}$) was quantified by destructively sampling leaves from the lower, middle, and upper canopy from sunrise until the canopy was dry as confirmed by visual observation of the absence of droplets. Wetness was calculated as the difference in water mass between wet and dried leaves normalized for leaf area.

Leaf apoplast NH_4^+ and H^+ concentrations were measured approximately biweekly using the vacuum infiltration technique of Husted and Schjoerring (1995). Leaf samples were taken from the upper canopy during late morning, after the canopy had dried, and extracts were composited until sufficient volume was collected for pH and NH_4^+ analyses. Duplicate composite samples were analyzed, typically consisting of 5 mL of sample in each (≈ 50 g fresh vegetation). Dilution of the apoplast during extraction was quantified by extracting leaves with indigo carmine and measuring the difference in absorbance at 610 nm (Ocean Optics Model USB2000 spectrometer, Dunedin, FL, USA) between the infiltrate and extracted sample. A 1 mL subsample was analyzed immediately for pH using a PHR-146 microelectrode (Lazar Research Laboratories, Inc., Los Angeles, CA, USA). The remaining sample was then analyzed in duplicate for NH_4^+ by ion chromatography (Dionex Model DX-120).

Leaf surface water consisting of dew and guttation droplets was collected on several occasions by direct syringe sampling and analyzed for pH and NH_4^+ using the methods described above. An artificial leaf droplet experiment was conducted on DOY 217 (LAI $\approx 1.8\, m^2 m^{-2}$) in which deionized water adjusted to a pH of 4.2 by addition of phosphorous acid was added to leaf surfaces as small droplets and recollected over a period of 5–35 min as a time series. The initial pH of 4.2 is consistent with the chemistry of local rainfall (National Atmospheric Deposition Program/National Trends Network, 2012). At the beginning of the experiment, approximately 50 mL of solution was quickly distributed via syringe among 20 green sunlit leaves selected randomly within a 10 m × 10 m section of the canopy. At each time interval, approximately 2 mL of the solution was retrieved from random locations. Aliquots of the composite sample at each time step were analyzed immediately for pH and frozen for later

analysis of dissolved ions, including potassium (K^+), magnesium (Mg^{2+}), and calcium (Ca^{2+}), by chromatography. The experiment was conducted between 10:00 and 13:00.

Soil samples were collected approximately weekly at 12 locations within 100 m of the NH_3 flux measurement tower: 6 locations to the north and south of the tower, respectively. At each location, three soil samples (0 to 5 cm depth) were taken at the mid-point and sides of the planting row (i.e., adjacent to plants). Samples were composited and subsamples were analyzed for NH_4^+, NO_3^-, H^+ and moisture. A 5-g subsample of field moist soil was extracted within 1 h of collection in 25 mL of 1M KCl. Extracts were frozen and later analyzed for NH_4^+ and NO_3^- by colorimetry (Lachat QuickChem Model 8000 Flow-Injection Autoanalyzer, Lachat Instruments, Loveland, CO, USA). Soil pH was measured within 1 h of sample collection in a 1:5 soil:deionized water mixture. Gravimetric soil moisture was determined by weight loss after heating 10 g of soil for 48 h at 60 °C. Particle size fraction and bulk density were also determined at 0–10, 10–20, and 20–30 cm layers using standard methods. Soil volumetric water was measured continuously at 10 cm and 20 cm depth using water content reflectometers (Model CS615, Campbell Scientific, Logan, UT, USA). Soil temperature averaged over 4–8 cm depth was measured continuously using chromel-constantan thermocouples (Campbell Scientific).

H^+ and NH_4^+ concentrations in the soil solution, leaf apoplast, and leaf surface water were used to calculate respective NH_3 compensation points (χ) according to

$$\chi = \frac{161\,500}{T} \exp\left(-\frac{10\,380}{T}\right) \frac{[NH_4^+]}{[H^+]}, \qquad (2)$$

where T is soil or air temperature in kelvin and H^+, NH_4^+, and χ concentrations are in $mol\, L^{-1}$ (Nemitz et al., 2000). χ is subsequently converted to units of $\mu g\, NH_3\, m^{-3}$. Plants may act as a source or sink for NH_3, depending on the difference between the atmospheric concentration and the gaseous concentration in the leaf substomatal cavity. The gaseous concentration in the leaf substomatal cavity is known as the stomatal compensation point (Farquhar et al., 1980). Emission occurs if the mole fraction of NH_3 in the atmosphere is lower than the stomatal compensation point, while uptake (deposition) occurs when the mole fraction of NH_3 in the atmosphere is higher than the stomatal compensation point. Compensation points for soil and leaf surface water can be similarly calculated from measured NH_4^+ and H^+ concentrations. The ratio of NH_4^+ to H^+ concentration in Eq. (2) is termed the emission potential (Γ), which is unitless and temperature independent.

3 Results and discussion

3.1 Data processing

Relative to the time-integrated manual denuder measurements, the AMANDA dataset is more complete with respect to temporal coverage and resolution and therefore is used as the primary dataset in the proceeding analysis of data quality and flux processes.

It is well known that the modified Bowen ratio technique is most uncertain under conditions of weak gradients and fluxes from which the eddy diffusivity is derived, particularly during periods of rapid stability transition such as evening and early morning. In the present study, eddy diffusivities were derived from the kinematic heat flux and temperature gradients. When both are near zero, the direction of the heat flux and temperature gradient may be opposite in sign, yielding a negative eddy diffusivity. Periods of negative eddy diffusivity account for $\approx 18\%$ of the total number of NH_3 gradient measurements ($N = 2294$), leaving a total of 1870 flux measurement periods for analysis. These remaining data were flagged according to a set of micrometeorological criteria to identify periods when the fluxes were subject to greater uncertainty due to limitations of the micrometeorological assumptions underlying the gradient method and fetch considerations. To indicate periods of limited turbulent mixing, data were flagged for wind speed (u) $< 0.5\,\mathrm{m\,s^{-1}}$, which corresponds to 22% of observations. As mentioned above, stability transition in the morning and afternoon is characterized by low kinematic heat fluxes and small temperature gradients. These periods were identified as having an Obukhov length $|L| < 0.2\,\mathrm{m}$, which corresponds to 9% of observations. Using the footprint model of Hsieh et al. (2000), fluxes were flagged if the corn field contributed $< 80\%$ of the flux at the upper height of the NH_3 concentration gradient. Owing to the large size of the field, only another 8% of observations failed this requirement after filtering for L. Periods in which the sampling tower fell within the aerodynamic footprint of the on-site mobile laboratory (wind direction $= 85$–$95°$) and when winds approached the sampling tower from the opposite side of the sample inlets (wind direction $= 355$–$5°$) were also flagged. These periods of potential flow obstruction collectively accounted for 3% of observations.

Accounting for periods of instrument maintenance and malfunction, as well as negative eddy diffusivities, flux data coverage between DOY 142 and 214 is 54%. Of these observations, 70% meet the meteorological criteria described above. Flagged data denote periods of greater uncertainty in the fluxes but were included in the following analyses.

3.2 Gradient detection limit and flux uncertainty

The quality of the fluxes was further assessed by estimating the percentage of observations above the operational gradient detection limit and total uncertainty in the flux. The
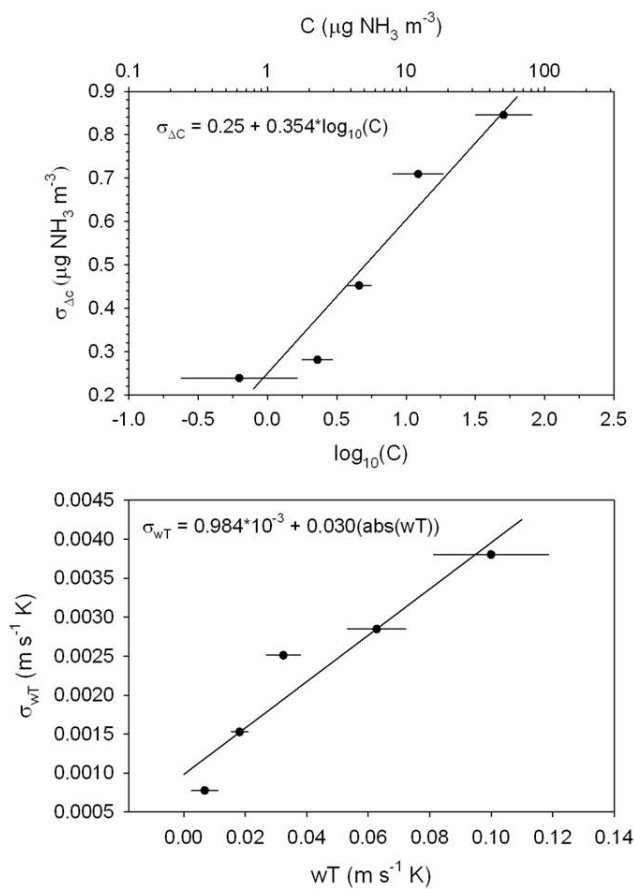
Fig. 1. Summary of relationships used to derive precision estimates of AMANDA NH_3 gradient ($\sigma_{\Delta c}$) and kinematic heat flux ($\sigma_{\overline{w'T'}}$) measurements from which the uncertainty of the modified Bowen ratio NH_3 flux was calculated. In the top graph, upper and lower x-axes represent NH_3 air concentration and log-transformed concentration, respectively. In the lower graph, the x-axis represents the kinematic heat flux. Symbols represent bin-wise average values, and error bars represent ± 1 standard deviation of x.

gradient detection limit was quantified as outlined by Wolff et al. (2010) based on the precision of the air concentration measured during periods in which the denuder sample boxes were collocated (i.e., cosampling periods). The residuals of an orthogonal linear regression of the concentrations measured by the two sample boxes represent random error in the air concentration. The standard deviation of the residuals provides a measure of the total precision of the concentration gradient ($\sigma_{\Delta C}$), which is a measure of the gradient detection limit (Wolff et al., 2010). To examine the relationship between $\sigma_{\Delta C}$ and air concentration, the observations were ordered by air concentration ($C = \mu g\,NH_3\,m^{-3}$) and segregated into 5 bins of $N = 45$ observations, from which $\sigma_{\Delta C}$ was calculated. As illustrated in Fig. 1, $\sigma_{\Delta C}$ increases linearly with the log-transformed air concentration. The resulting function of $\sigma_{\Delta C}$ versus C was used to predict the gradient detection limit for each flux observation. Using this approach, 70%

($N = 1292$) of the observed 30-min average gradients from which the flux was determined were above the gradient detection limit.

Uncertainty in the flux (σ_F) was quantified as the combination of uncertainty in the concentration gradient ($\sigma_{\Delta C}$) and eddy diffusivity for sensible heat (σ_{K_h}) following Gaussian error propagation (Walker et al., 2006):

$$\sigma_F = \sqrt{\left(\sigma_{K_h} \cdot \Delta C\right)^2 + \left(\sigma_{\Delta c} \cdot K_h\right)^2}. \tag{3}$$

Uncertainty in the concentration gradient was determined as described above, and uncertainty in the eddy diffusivity (K_h) was determined from the uncertainty in the temperature gradient ($\sigma_{\Delta T}$) and the kinematic heat flux ($\sigma_{\overline{w'T'}}$):

$$\sigma_{K_h} = \sqrt{\left(\frac{\sigma_{\overline{w'T'}}}{\Delta T}\right)^2 + \left(\frac{\left(\overline{w'T'}\right)\sigma_{\Delta T}}{(\Delta T)^2}\right)^2}. \tag{4}$$

For consistency, $\sigma_{\Delta T}$ and $\sigma_{\overline{w'T'}}$ were determined using the orthogonal least squares regression procedure described above. $\sigma_{\overline{w'T'}}$ was derived from collocated measurements of $\overline{w'T'}$ in which duplicate R. M. Young sonic anemometers were vertically matched in height and separated horizontally by approximately 0.5 m. To assess the potential relationship between the precision and magnitude of the heat flux, absolute values of $\overline{w'T'}$ were ordered and segregated into 5 bins of $N = 30$ observations. The linear relationship between the mean and standard deviation of the bin-wise heat fluxes (Fig. 1) was then used to predict $\sigma_{\overline{w'T'}}$ for each $\overline{w'T'}$ observation in the NH_3 flux dataset. Similarly, $\sigma_{\Delta T}$ was derived from collocated duplicate thermocouple measurements of air temperature (T). $\sigma_{\Delta T}$ did not exhibit a dependence on T; therefore, the overall standard deviation of the orthogonal least squares residuals ($\sigma_{\Delta T} = 0.024\,\mathrm{K}$, $N = 104$) was used in the flux uncertainty calculation (Eq. 4). Following this approach, the median error of the flux (i.e., $(\sigma_F / F) \cdot 100$) is 43 % considering only chemical gradients that are above the detection limit. Uncertainty is greatest at night when the heat flux and temperature gradient are small (Fig. 2). During these periods, the median hourly uncertainty ranges from 65–85 %. Hourly median uncertainty is lowest between 09:00 and 14:00 (25–30 %) when fluxes of heat and NH_3 are large. Median uncertainty for all fluxes, including chemical gradient below detection limit, is 59 %. However, this number represents periods of large uncertainty at night corresponding to fluxes near zero. Median uncertainty of all daytime fluxes only, which captures the majority (> 90 %) of the total daily flux, is 46 %.

3.3   Comparison of measurement techniques

AMANDA air concentrations were compared to manual denuder measurements comprising three sets of data: 12-h (D_{12}) integrated samples collected at a single height, 2–3 h
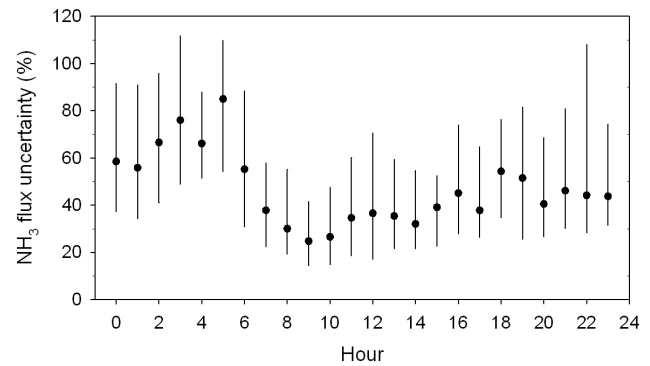

Fig. 2. Hourly median uncertainty of the modified Bowen ratio flux measured with the AMANDA. Error bars represent the interquartile range.

samples from the in-canopy profile system (D_{IC}) and 2-h samples from the second Bowen ratio system (D_{BR2}). Precision of the D_{IC} and D_{BR2} systems, determined as the median relative percent difference of duplicate measurements, was 4.6 % ($N = 45$) and 11.6 % ($N = 30$), respectively. Precision of the D_{12} integrated samples is ~5 % (Robarge et al., 2002).

Prior to comparison, concentrations were normalized using the linearized vertical concentration gradient ($dC/d\ln z$) to adjust for differences in measurement heights. For the D_{12} comparison, the AMANDA gradient was interpolated for the D_{12} height. For the D_{IC} comparison, the concentration of the lower AMANDA denuder was compared directly to the uppermost denuder in the canopy profile system. AMANDA and D_{BR2} were compared by normalizing both gradients to 1 m. Data were then filtered for 80 % completeness of AMANDA coverage for a given period of denuder sampling, yielding 112 observations for comparison. Linear regression analysis of AMANDA versus manual denuder concentrations (Fig. 3) yielded a slope of 0.96 and a statistically non-significant ($P = 0.1$) intercept of $-0.19\,\mu\mathrm{g\,m^{-3}}$, indicating good overall agreement between methods. Scatter in the data is attributed to spatial variability in emissions, which would make agreement between methods sensitive to horizontal and vertical separation, particularly following fertilization or periods during which the flux changed rapidly.

Comparison of AMANDA versus manual denuder fluxes is limited to only 13 periods during which AMANDA coverage was complete. Given the difficulties inherent in measuring NH_3 fluxes and large natural variability in the data, such a limited dataset precludes rigorous comparison. However, mean fluxes were 64.0 and 67.0 $\mathrm{ng\,NH_3\,m^{-2}\,s^{-1}}$ for the AMANDA and manual denuder systems, respectively. Using the nonparametric Wilcoxon rank sums test, the means are not significantly different at the 10 % level, suggesting that on average large systematic differences between the two techniques are not expected.
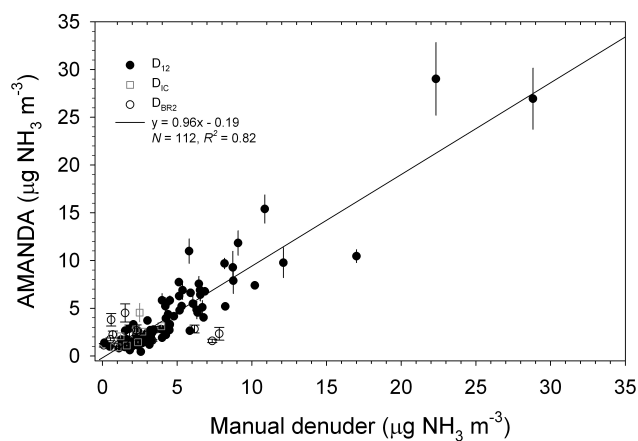
Fig. 3. Comparison of AMANDA NH_3 concentration measurements to 12-h (D_{12}) integrated samples, 2–3 h samples from the in-canopy profile system (D_{IC}) and 2-h samples from the second Bowen ratio system (D_{BR2}). Concentrations were normalized to a common level using the linearized concentration gradient ($dC/d\ln z$) to account for differences in measurement heights. Error bars represent ±1 standard deviation of the mean half-hourly AMANDA measurements.

3.4 Fluxes

Cumulative fluxes (Fig. 4a) were calculated over a period of approximately 10 weeks from the point of UAN fertilization (DOY 149) to DOY 214. To avoid biasing the results toward hours of the day during which there are a higher number of valid observations, which may occur if daily mean or median fluxes are used, cumulative fluxes were calculated from mean and median diurnal flux profiles. To capture the general temporal features of the flux following fertilization, diurnal profiles were summarized by four periods (Fig. 4a): DOY 149 to 161, DOY 162 to 172, DOY 173 to 180, and DOY 181 to 214. Using this approach, daily mean and median NH_3 fluxes yield cumulative total N losses of 8.3 % and 6.1 %, respectively, of the $134\,kg\,N\,ha^{-1}$ surface applied as UAN. For nitrogen containing solutions, including surface applied UAN, an NH_3–N emission factor of 8 % has been used in recent US emission inventories (Geobes et al., 2003; ECETOC, 1994. This value is consistent with the controlled experiments of Watson et al. (2008), which examined fractional NH_3–N loss (≈ 8 % averaged over all treatments) from UAN solutions in a variety of soil types at different temperatures.

The urease inhibiting action of nBTPT, the active ingredient in Agrotain®, has been shown to reduce and delay NH_3 volatilization from urea in a number of field trials (Watson et al., 1994; Rawluk et al., 2001). NH_3 emissions from UAN + nBTPT have been studied less extensively. However, field (Chadwick et al., 2005) and laboratory (Watson et al., 2008) experiments indicate reduced and delayed emissions relative to UAN solutions without nBTPT, though % reduction of NH_3 volatilization is lower than observed for
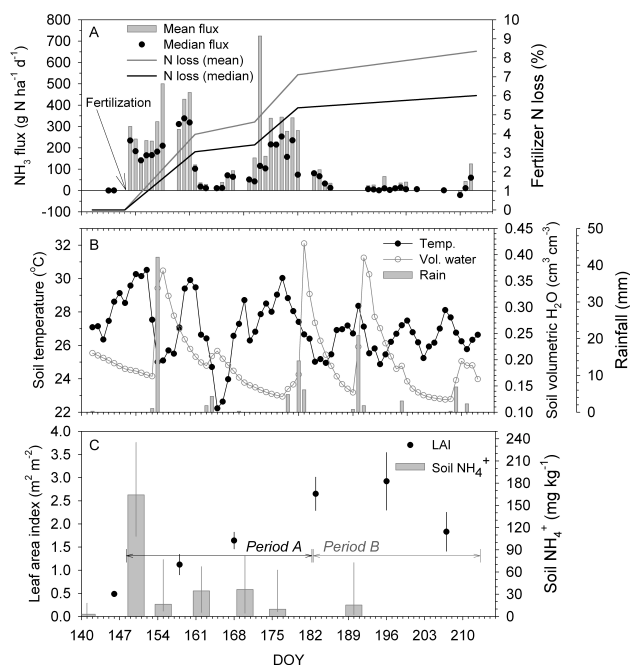
Fig. 4. Daily mean and median NH_3 fluxes along with equivalent % N loss of applied fertilizer **(A)**; daily average soil temperature averaged over 4–8 cm depth, soil volumetric water at 10 cm depth, and rainfall **(B)**; and single-sided leaf area index (LAI) and soil extractable NH_4^+ concentrations (0–5 cm depth) **(C)**. Error bars in bottom graph represent ±1 standard deviation of the mean. DOY represents the Julian day of the year.

urea + nBTPT owing to a lower % nitrogen associated with urea in UAN. In field trials on tillage soils, NH_3 volatilization from surface applied UAN + nBTPT was 44 % lower, on average, than volatilization from UAN only (Chadwick et al., 2005) over a period of 21 days after fertilization. Reductions were slightly larger in laboratory experiments, averaging 65 % across soil types, nBTPT concentration, and soil temperature (Watson et al., 2008), also over a 21 day period. Reducing the 8 % emission factor assumed for UAN solutions by 44 % and 65 % yields an expected range of percent NH_3–N loss from UAN + nBTPT solutions of 5.3 % and 2.8 %, respectively. Our estimates of 8.3 % (6.1 %) total loss and 4.5 % (3.4 %) at 21 days from fertilization derived from daily mean(median) fluxes are consistent with this range of values. Note that the experiments of Watson et al. (2008) did not account for the recapture of soil emissions by overlying vegetation, which is in contrast to the net fluxes presented here. Though LAI (Fig. 4c) was still relatively low (≈ 1.75) at 21 days after fertilization, soil emissions were likely higher than the net canopy-scale emissions from which % N loss was calculated.

The majority of the cumulative flux occurred in two distinct periods (Fig. 4a). Fluxes increased immediately upon the completion of fertilization (DOY 149) and remained elevated for a period of several days. A decrease in emissions

during the second week after fertilization was followed by a second period of increased emissions beginning in the third week after fertilization and lasting for approximately one week. We primarily attribute this temporal pattern to fertilizer characteristics. The emission pulse immediately following fertilization is likely primarily associated with the NH_4^+ fraction of the UAN fertilizer. The highest daily median fluxes were observed following the first post-fertilization rainfall (DOY 153/154). Emissions decreased dramatically as soil temperatures decreased in response to the passage of a cold front on DOY 160 after which overcast skies persisted for a period of several days. The second period of elevated emission (DOY 172–180) developed as the soil warmed for several days following a light rainfall on DOY 162 (Fig. 4b). This delayed second emission pulse likely reflects the urease inhibiting properties of the nBTPT (Agrotain), which has been shown to delay hydrolysis of urea for up to 3 weeks in some soils (Giaocchini et al., 2002).

The observed temporal pattern of emissions is to some extent supported by the corresponding pattern of soil extractable NH_4^+ (0–5 cm depth) concentrations (Fig. 4c). As expected, soil NH_4^+ concentrations were highest immediately following fertilization (DOY 149). The rainfall on DOY 153/154 likely moved some fraction of the fertilizer downward into the soil profile, potentially suppressing emission during the first week following fertilization relative to what would have been observed in the absence of rain. NH_4^+ concentrations (0–5 cm) were much lower a week after fertilization and increased over the next two weeks before gradually decreasing over the remainder of the growing season. The apparent increase in NH_4^+ between DOY 154 and 168 may reflect the conversion of urea to NH_4^+ and the decreasing efficiency of the urease inhibitor with time, which in combination with warming of the soil stimulated the second period of emissions.

To examine the temporal variability of fluxes in more detail, data were divided into two periods. The first period includes DOY 149–180 (period A), during which the effects of fertilization are distinct. The second period covers DOY 181–213 (period B), during which the canopy reached maximum LAI (Fig. 4c) and the effects of fertilization on the canopy-scale flux had diminished. Fluxes from both periods are summarized in Table 1 along with soil, vegetation, and meteorological measurements. During period A, 53 % of the variability in daily median fluxes is explained by a linear combination of soil temperature (38 %) and volumetric water (15 %) at the 10 cm soil depth. Fluxes are positively correlated with both variables. Consistent with other studies, fluxes tended to increase exponentially with temperature (Roelle and Aneja, 2002), which results from the temperature dependence of the gas/aqueous partitioning of NH_3 in the soil pore water (Dawson, 1977) through Henry's law. The rate of urea hydrolysis and subsequent production of NH_4^+ increases with increasing soil moisture (Vlek and Carter,

1983), while the resistance to transfer of NH_3 gas through the soil profile decreases (Moldrup et al., 1999). In combination, these processes yield a positive correlation between soil moisture and NH_3 flux, though their relative importance changes with time after fertilization as the effectiveness of the urease inhibitor decreases. Interpretation of the correlation between soil moisture and NH_3 emission during this period is therefore not straightforward.

At the diurnal timescale, maximum hourly average fluxes of $\approx 700\, \mathrm{ng\, N\, m^{-2}\, s^{-1}}$ occurred near mid-day, coincident with the daily maximum in friction velocity (u_*, Fig. 5). Linear correlation with friction velocity explains 31 % of the variability in log-transformed half-hourly fluxes, which are also positively correlated with air temperature and soil temperature after accounting for their respective collinearity with friction velocity. Correlation with air temperature explains more of the flux variability (11 %) than soil temperature (6 %), suggesting that the NH_3 source is very near the soil surface during this period. Friction velocity and temperature are linked through the compensation point. Large u_* flushes NH_3 out of the canopy, promoting more emission resulting from the compensation point, and higher temperatures correspond to higher compensation points. While including interaction terms for u_* and temperature in the regression procedure should control for most of this collinearity, in reality the total flux variability may be more evenly partitioned between these two variables. Soil volumetric water does not explain a statistically significant fraction of the variability in half-hourly fluxes.

Ammonia air concentrations are generally higher at night when the boundary layer is shallow, though concentrations increase rapidly in the morning with the post-sunrise increase in the momentum flux. This spike in concentration, which is accompanied by an emission pulse, likely represents the upward mixing of NH_3 that accumulates near the ground (i.e., below the lowest NH_3 measurement height) under calm nighttime conditions (Bash et al., 2010) and emissions from drying moisture on the soil surface. This period of elevated concentration in the morning coincides with the drying of the surface and rapid decline in relative humidity (RH) (Fig. 5). The latter point is discussed in more detail below.

During period B, 5 to 10 weeks after fertilization, net emission was still observed though mid-day peak fluxes had declined to $\approx 125\, \mathrm{ng\, N\, m^{-2}\, s^{-1}}$ and day-to-day variability of the net canopy-scale flux was not as well correlated with soil temperature or soil moisture. At the diurnal timescale, fluxes were again larger during the day when friction velocity was high. A prominent feature of the diurnal pattern is a peak in the NH_3 air concentration and emission flux at approximately 09:00. This period coincides with surface layer mixing after sunrise as wind speed and friction velocity increased as well as drying of the surface (Fig. 5). This pattern likely results from a combination of venting of the canopy and release of NH_3 from moisture that accumulates overnight at the soil surface (e.g., Sutton et al., 1998). This process and

Table 1. Summary of NH_3 fluxes ($ng\,m^{-2}\,s^{-1}$), NH_3 concentration at $(z - d) = 1\,m$ ([NH_3], $\mu g\,m^{-3}$), canopy temperature (T_c, °C), soil temperature averaged over 4–8 cm depth (T_{soil}, °C), wind speed at $z = 3.5\,m$ (U, $m\,s^{-1}$), soil volumetric water at 10 cm depth (H_2O_{vol}, $cm^3\,cm^{-3}$), NH_4^+ concentration in the leaf apoplast solution (NH_4^+)$_s$, leaf surface water (NH_4^+)$_d$, and soil pore water (NH_4^+)$_{soil}$ (μM), along with pH and emission potential ($\Gamma = NH_4^+/H^+$) of the corresponding media.

			Mean	Median	S.D.	Max.	Min.	N
	Air	NH_3 Flux	339.2	147.8	601.7	6906	−42.5	1051
		[NH_3]	10.3	8.4	7.2	61.2	1.3	1051
		U	1.3	1.1	0.9	5.7	0	1523
	Vegetation	T_c	24.6	23.9	5.5	44.7	13.7	1394
		(NH_4^+)$_s$	78.6	69.9	43.2	158.0	26.9	8
		pH_s	6.35	6.40	0.14	6.50	6.10	8
		Γ_s	184.5	153.5	130.1	451.9	76.5	8
Period A (DOY 149–180)		(NH_4^+)$_d$	52.9	53.9	4.9	58.9	45.6	5
		pH_d	7.6	7.9	0.7	8.1	6.6	5
		Γ_d	3768.3	4565.0	3058.6	6749.5	45.6	5
	Soil	T_{soil}	27.3	26.7	4	38.5	19.4	1536
		H_2O_{vol}	0.2	0.18	0.06	0.45	0.13	1530
		(NH_4^+)$_{soil}$	54 609.1	31 689.7	76 487.6	454 454.3	868.4	60
		pH_{soil}	6.41	6.43	0.58	7.91	5.14	60
		Γ_{soil}	219291.0	51 035.3	446 089.4	2 523 893.0	2288.4	60
	Air	NH_3 Flux	61.4	10.2	185.5	3125.4	−230.4	725
		[NH_3]	2.2	1.7	1.7	18.3	0.3	725
		U	1	0.8	0.7	4.6	0	1384
	Vegetation	T_c	25.3	25.1	5.1	43.1	13.1	1251
		(NH_4^+)$_s$	119.2	91.1	89.1	367.7	40.0	17
		pH_s	6.10	6.16	0.21	6.38	5.71	17
		Γ_s	148.3	139.4	93.4	401.9	33.2	17
Period B (DOY 181–213)		(NH_4^+)$_d$	35.6	34.4	35.9	166.1	0.6	29
		pH_d	8.02	8.05	0.44	8.67	7.36	22
		Γ_d	5001.0	4516.5	4924.4	19911.7	141.2	22
	Soil	T_{soil}	26.4	26.2	2.4	34.2	21.2	1522
		H_2O_{vol}	0.2	0.17	0.08	0.54	0.12	1522
		(NH_4^+)$_{soil}$	34 735.8397	3373.847	74 277.76	26 3061.7	462.387	23
		pH_{soil}	6.56	6.57	0.62	7.68	5.50	24
		Γ_{soil}	11 1922.8	14 722.7	210 607.0	770 670.3	179.9	23

the variability of the fluxes during period B are further explored below through an examination of the in-canopy NH_3 source/sink characteristics and soil/vegetation chemistry.

3.5 Vegetation and soil emission potentials

3.5.1 Leaf apoplast

Over the course of the growing season, (Fig. 6), apoplast NH_4^+ concentrations decreased gradually after fertilization until the onset of senescence ($\approx$ DOY 200) at which time NH_4^+ concentrations increased to levels observed just after fertilization. While apoplast extractions were performed only on green leaves during the senescing period, it is possible that the chemistry of the apoplast solution was influenced to some extent by cellular breakdown. Results during this period should therefore be interpreted cautiously. Apoplast pH exhibited the opposite pattern, increasing after fertilization

until the onset of senescence, then decreasing slightly. The net effect was a relatively constant apoplast emission potential ($\Gamma_s = NH_4^+/H^+$) though mean and median Γ_s were slightly higher during period A, after fertilization, compared to period B (Table 1). In general, the emission potential of the leaf apoplast was much lower than the soil pore or leaf surface water (Table 1). Over the typical range of daytime temperatures (25–35 °C), the overall median Γ_s (146) corresponds to stomatal compensation points (χ_s) in the range of 1–3 $\mu g\,NH_3\,m^{-3}$ (Fig. 7).

The range of measured apoplast Γ_s values (33–452) overlaps with the cuvette measurements of Farquhar et al. (1980) for corn, but observations from this study are lower than the average Γ_s (1186 ± 395) inferred from micrometeorological measurements by Harper and Sharpe (1995). Massad et al. (2010) point out that extraction techniques, such as employed in this study, generally yield lower estimates of
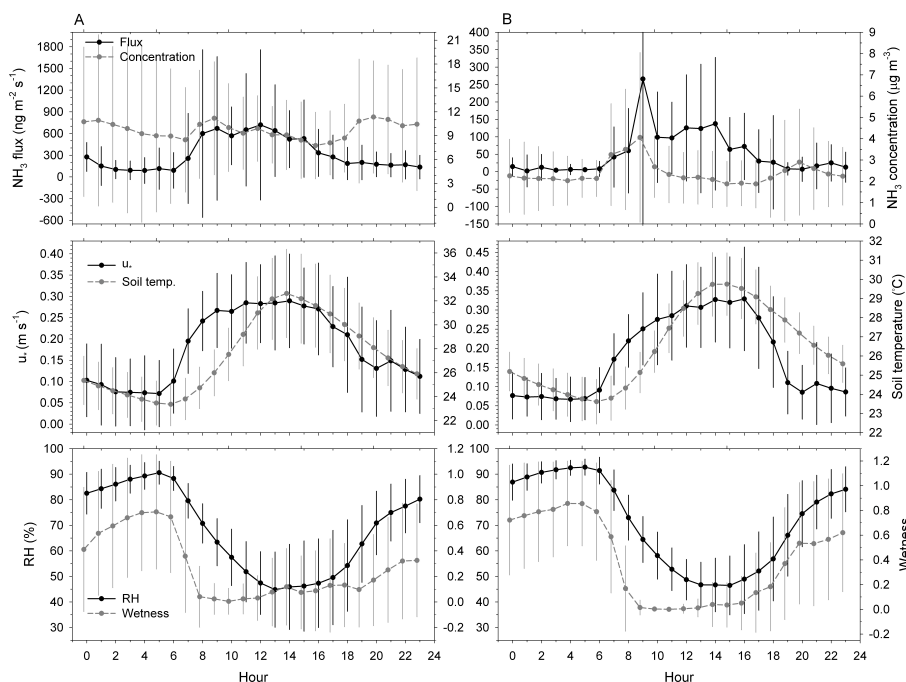
Fig. 5. Mean hourly NH_3 flux, NH_3 air concentration at $(z - d) = 1\,m$, friction velocity (u_*), soil temperature averaged over 4–8 cm depth, relative humidity (RH), and leaf wetness for Periods A and B. Leaf wetness represents the fraction of the hourly period during which the leaf wetness sensor indicated that moisture was present. Error bars represent ± 1 standard deviation of the mean.

Γ_s compared to gas exchange approaches, possibly as a result of regulation of H^+ and NH_4^+ post-collection of the leaf material and during extraction or because gas exchange is dominated by localized hotspots. Differences between our results and those of Farquhar et al. (1980) and Harper and Sharpe (1995) may also be related to fertilizer amount and plant growth stage.

3.5.2 Leaf surface water

The leaf surface water, composed of dew and guttation, exhibited mean and median Γ_d of 4327 and 4502, respectively. NH_4^+ concentrations were approximately a factor of 2 lower on average than concentrations measured in the leaf apoplast, ranging from 0.6 to 166 μM. The much higher emission potential relative to the apoplast was instead a result of higher pH, which ranged from 6.6 to 8.7. The observation of high pH in natural dew and guttation was further explored in a controlled experiment in which deionized water, adjusted to a pH of 4.2 by addition of phosphorous acid, was added to green sunlit leaves as small droplets and re-collected over a period of 5–35 min as a time series.

The pH of the artificial leaf droplets increased rapidly and appeared to reach a maximum increase of 2 to 4 pH units within 30 min; droplets applied to a clean surrogate surface maintained a constant pH (Fig. 8). Final pH values after 35 min were slightly lower than natural dew droplets and guttation but confirmed a large neutralizing capacity of the

leaf surface. While consistent temporal trends in dissolved ions were not clear from this limited dataset, general increases in K^+, Mg^{2+} and Ca^{2+} were observed, with very high concentrations of K^+ noted in a few samples (Table 2). The high concentrations of these base cations suggest two possible mechanisms responsible for the high observed pH, the first being H^+ exchange. As explained by Mecklenburg et al. (1966), water in dew and guttation dissolves CO_2 from the atmosphere to form carbonic acid, which then dissociates, releasing H^+. These protons are exchanged with base cations through the cuticle on sites within the leaf cell wall to form alkaline carbonates, which may remain in solution or precipitate back to the cuticle surface. Second, solubilization of pre-existing alkaline particles, from sources such as soil, on the cuticle would also increase the pH (Hutchinson et al., 1986). This process is very likely, given that the system is composed of a short canopy over tilled soil that was relatively dry for extended periods of time during the growing season. Furthermore, the presence of soil particles on the leaves was visually observed, particularly in the lower canopy. Our measurements were not sufficiently detailed to resolve possible variations in pH with vertical position in the canopy, though a higher surface neutralizing capacity of leaves in the lower canopy is expected given that rain is more likely to clean leaves in the upper canopy more completely. Interaction of other trace compounds with the water layers will further complicate the leaf water chemistry (Flechard et al., 1999; Burkhardt et al., 2009).
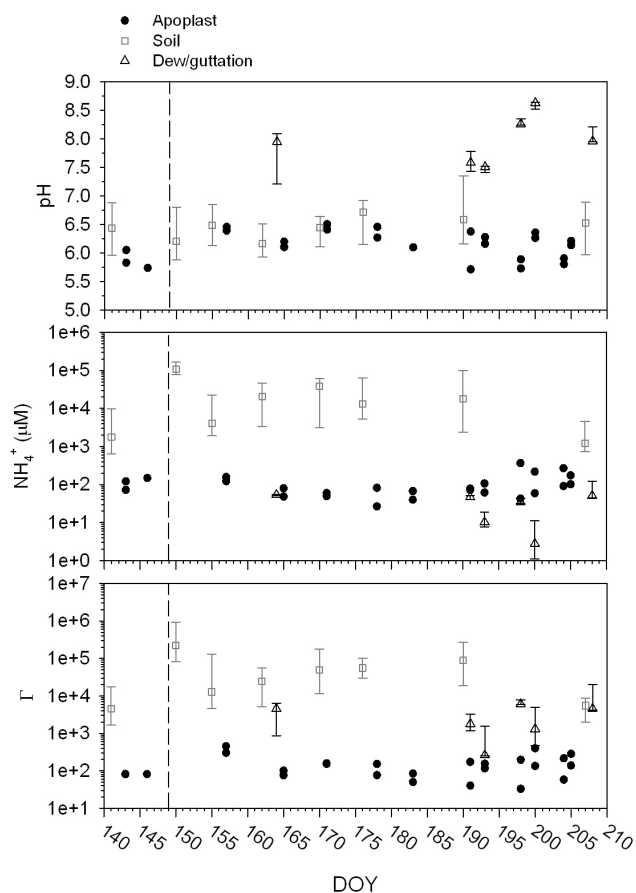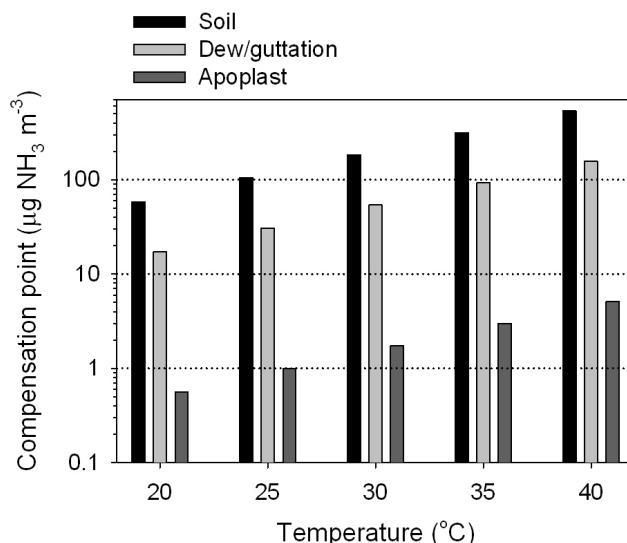
Fig. 6. Time series of pH, NH_4^+ concentration, and emission potential ($\Gamma = NH_4^+/H^+$) of the soil pore water, leaf apoplast and leaf surface water consisting of dew and guttation. DOY represents Julian day of the year. Vertical dashed line represents date of UAN fertilizer application. Symbols represent median values, and error bars represent interquartile range.

Table 2. Summary of pH and base cation concentrations ($\mu g\,L^{-1}$) measured during controlled leaf droplet experiments. S.D. represents standard deviation, and N represents number of samples.

	Mean	Median	S.D.	Max.	Min.	N
pH	6.83	6.79	0.83	8.34	5.70	12
K^+	23 074	2150	46 852	135 950	530	12
Mg^{2+}	2360	2200	1499	5300	160	12
Ca^{2+}	3340	2450	2593	9250	40	12

High neutralizing capacity of leaf surface droplets has also been observed for leaves of other crops (Hutchinson et al., 1986), particularly species with wettable leaf surfaces. However, the pH of leaf surface water on trees and grasses is typically lower, in the range of 3.5 to 6.5 (Hutchinson et al., 1986; Burkhardt and Eiden, 1990; Burkhardt et al., 2009). In general, measurements of leaf droplet pH reported in the literature are highly variable, which results not only from

Fig. 7. Compensation point of soil pore water, leaf surface water (dew/guttation) and leaf apoplast derived from measured NH_4^+ and H^+ concentrations as a function of temperature.
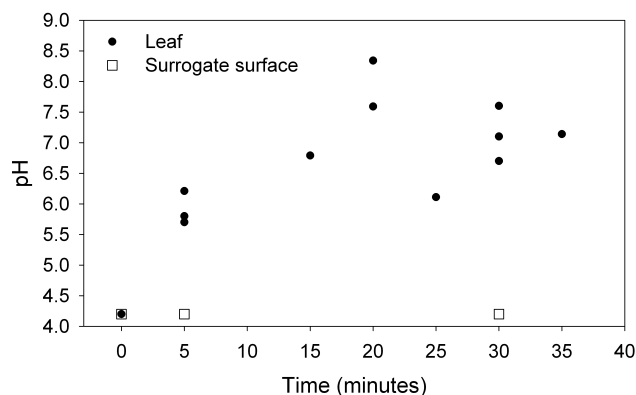
Fig. 8. Time series of pH during controlled leaf droplet experiment. Black dots represent pH of droplets applied to leaves, and open squares represent pH of droplets applied to clean Teflon surface. Droplets of pH 4.2 consisting of deionized water and phosphorous acid were applied at $t = 0$.

vegetation characteristics but also the chemical characteristics of dry deposition to leaf and needle surfaces. High pH corresponds to a high emission potential, with Γ_d producing compensation points for leaf surface water (χ_d) of 10 to $30\,\mu g\,NH_3\,m^{-3}$ over the range of typical observed nighttime temperatures (18–28 °C, Fig. 7). As described in the following section, NH_3 concentrations within the vegetation canopy were highest immediately above the soil surface and decreased exponentially with height. During the four periods in which in-canopy concentrations were measured at night and under wet or partially wet canopy conditions in the early morning, concentrations at 10 cm above the soil were $<10\,\mu g\,NH_3\,m^{-3}$ (2.7 to 7.8), indicating that, late in the

growing season, leaf wetness would not have played a large role in the recapture of soil emissions at night.

To explore further the role of canopy wetness in the net canopy-scale flux, nighttime fluxes were compared between periods when the canopy was wet versus dry. At night, stomata are closed and the leaf level exchange should therefore be dominated by cuticular processes. To normalize the comparison for turbulence conditions, data were filtered to include only $0.01 < u_* < 0.2 \, \mathrm{m \, s^{-1}}$, which produced approximately equivalent mean u_* between the dry and wet periods. Comparison of leaf-level processes also assumes that differences between soil emissions are negligible. Because soil emissions should be larger immediately following rain events (i.e., high soil volumetric water content), data were also filtered to exclude days on which rain occurred. As shown in Table 3, net canopy-scale emissions at night were larger when the canopy was wet, indicating that the wetting of the canopy, and the accompanying high pH of the surface water, increased the cuticular resistance to NH_3 uptake and reduced the capacity of the canopy to recapture soil emissions. Because air concentrations were similar between wetness categories, differences in fluxes translate into differences in exchange velocities (V_e = flux/concentration), with higher exchange velocities observed when the canopy was wet. Comparing periods, the percent difference between the mean fluxes during dry versus wet periods is much larger during period B, later in the growing season, compared to period A. This likely reflects the lower overall leaf surface area during period A and higher in-canopy concentrations of NH_3 resulting from larger soil emissions, which may exceed χ_d more frequently compared to period B. It is also possible, however, that soil emissions were larger during period B wet conditions due to higher soil volumetric water. During period A, soil volumetric water content was similar during wet and dry canopy conditions (Table 3). Differences in canopy-scale fluxes are therefore not likely due to differences in soil emissions. During period B, a difference in soil volumetric water between canopy wetness categories persists even after eliminating days on which rain occurred, with higher soil volumetric water content corresponding to wet canopy periods. We can not rule out the possibility that the higher fluxes during wet canopy conditions were partly due to higher soil emissions.

The relationship between leaf wetness and flux described above differs from previous studies, in which leaf wetness typically reduces the cuticular resistance to NH_3 deposition (see review of Massad et al., 2010). The most notable contrast to previous work is the very high pH of leaf surface droplets observed in the present study, with corresponding high Γ_d. Additional measurements are needed to assess the extent to which our observations of high surface water pH are site specific (i.e., driven by soil particles persisting on leaf surfaces) rather than a general feature of corn plants (i.e., driven by characteristics of transcuticular ion exchange). Furthermore, the extent to which bulk sampling of leaf surface

Table 3. Summary of fluxes (ng $NH_3 \, m^{-2} \, s^{-1}$), NH_3 concentration at $z - d = 1 \, m$ ($\mu g \, m^{-3}$), exchange velocity (V_e, cm s^{-1}), u_* (m s^{-1}), and soil volumetric water (S.V.W., cm^3 cm^{-3}) during wet and dry night-time conditions for periods A and B. Data were filtered to include only $0.01 < u_* < 0.2$, which established approximately equal u_* between wetness categories, thereby essentially normalizing the comparison for turbulence conditions. Data were also filtered to exclude days on which rain occurred. S.D. and N represent standard deviation and number of observations, respectively.

		Period A Dry	Period A Wet	Period B Dry	Period B Wet
Flux	Mean	82.9	133.9	0.5	10.7
	S.D.	122.8	224.9	21.3	27.6
	Median	36.5	36.6	0.9	1.9
NH_3	Mean	11.6	12.8	2.0	2.3
	S.D.	7.6	11.4	1.3	1.6
	Median	9.2	7.6	1.6	1.7
V_e	Mean	0.77	1.08	0.03	0.34
	S.D.	1.08	1.60	1.15	0.81
	Median	0.37	0.43	0.05	0.11
u_*	Mean	0.08	0.08	0.07	0.06
	S.D.	0.05	0.04	0.05	0.04
	Median	0.07	0.07	0.05	0.05
S.V.W	Mean	0.19	0.18	0.15	0.22
	S.D.	0.06	0.04	0.02	0.05
	Median	0.16	0.17	0.14	0.20
N		170	118	87	155

water represents the cuticular NH_3 exchange characteristics of the entire canopy is unknown. It is possible that bulk sampling does not resolve the spatial variability in H^+ and NH_4^+ concentrations that also affect the net canopy-scale flux. Microscopic (invisible) leaf water layers control the cuticular exchange at high RH when no visible leaf water is present, but their chemistry cannot be measured directly for comparison. While our comparison of fluxes during wet and dry periods suggests that the bulk chemistry of the leaf surface water is linked to the net canopy-scale flux, the representativeness of the bulk measurements with respect to overall cuticular exchange characteristics is uncertain.

In addition to the uncertainties described above, there are two notable limitations of this assessment. First, U and u_* are typically low at night in Eastern North Carolina during the summer. The mean u_* values in Table 3 are $< 0.1 \, \mathrm{m \, s^{-1}}$, corresponding to conditions of small heat fluxes and temperature gradients under which the modified Bowen ratio technique becomes highly uncertain (Fig. 2). Second, the majority of the leaf droplet measurements were collected late in the growing season (Fig. 6), which precludes a robust characterization of potential temporal variability of leaf surface

water chemistry as the canopy grew. Γ_d was similar during periods A and B (Table 1).

3.5.3 Soil

The soil pore solution exhibited mean and median Γ_{soil} values of 120 000 and 15 400, respectively, which is consistent with the observations from fertilized soils compiled by Massad et al. (2010). Over the range of observed soil temperatures (20–40 °C), the median Γ_{soil} corresponds to soil compensation points (χ_{soil}) in the range of 60–500 μg NH_3 m^{-3} (Fig. 7). Γ_{soil} was considerably higher during period A compared to period B (Table 1), reflecting the high concentrations of soil NH_4^+ measured immediately after fertilization. Over the course of the growing season, variability in Γ_{soil} was primarily driven by variability in soil NH_4^+, while soil pH remained relatively constant throughout the growing season. Soil NH_4^+ concentrations were highest immediately following fertilization and decreased dramatically between the first and second sampling periods post-fertilization (Fig. 6), most likely in response to volatilization losses of NH_3 from the NH_4^+ fraction of the UAN solution and heavy rainfall on DOY 154, which would have diluted the surface fertilizer and moved it down into the soil profile. NH_4^+ concentrations then increased for a period of 2 to 3 weeks, likely as a result of conversion of urea to NH_4^+ as the urease inhibiting efficiency of the Agrotain nitrogen stabilizer declined. NH_4^+ decreased late in the growing season, after the onset of canopy senescence, to pre-fertilization levels.

3.6 In-canopy source/sink processes

3.6.1 Net canopy-scale fluxes

An intensive in-canopy experiment was conducted between DOY 187 and 213, capturing peak LAI (Fig. 4), to quantify the relative importance of the soil and foliage NH_3 exchange processes with respect to the net canopy-scale flux. The source/sink profile within the canopy was estimated from measured vertical NH_3 concentration profiles and turbulence parameters using a first-order analytical closure model, which is described in detail by Bash et al. (2010). A brief description of the model is included as Supplemental Material.

In-canopy concentration profiles consisting of 15 measurement periods are summarized by time of day in Fig. 9. All profiles followed a pattern of highest concentrations near the soil surface, decreasing rapidly with height in the lower quarter of the canopy, then more slowly to the top of the canopy. Based on the consistency of the profile shapes, the soil appeared to still be a constant source of NH_3 at this stage of the growing season. The shape of the profiles was driven by a combination of turbulent mixing within the canopy and the concentration of NH_3 just above the soil surface. Bash et al. (2010) showed that the source/sink profiles were indica-
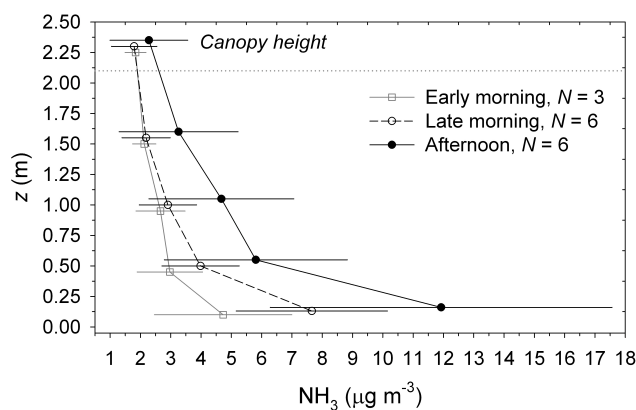
Fig. 9. In-canopy NH_3 concentration versus measurement height above the ground (z). Symbols represent the mean, and error bars represent ±1 standard deviation of the mean. N represents number of observations at each height. Lines connecting observations are included only as a visual aid. "Early morning" includes profile measurement periods ending before 09:00, "late morning" profile measurement periods ending between 09:00 and 13:00, and "afternoon" profile measurement periods ending between 13:00 and 18:00.

tive of emission from the soil and recapture of a varying fraction of emissions by the overlying canopy. The modeled average flux from the soil was 155 ng m^{-2} s^{-1}, and the net flux to the atmosphere was 37 ng m^{-2} s^{-1}, which agreed reasonably well with the micrometeorological flux measurements during the corresponding in-canopy measurement periods. The average total flux to the foliage (cuticular plus stomatal fluxes) was −118 ng m^{-2} s^{-1}, equivalent to 76 % of the average soil flux. The slight difference between our value of 76 % canopy recapture and the value of 73 % reported by Bash et al. (2010) reflects the use of average fluxes in the present analysis. Our results are consistent with other studies that have shown the recapture of NH_3 emissions from fertilized soil by the overlying crop canopy (Harper et al., 2000; Nemitz et al., 2000).

3.6.2 Soil flux

The flux from the ground (F_g) is driven by the difference between the soil (χ_{soil}) and canopy (χ_c) compensation points, the resistance to diffusion through the soil profile (R_{soil}), the resistance to diffusive transport across the air-side laminar boundary layer at the soil surface (R_{bg}) and the resistance to turbulent transfer within the canopy (R_{inc}), all of which can be viewed within a resistance modeling framework:

$$F_g = \frac{\chi_{soil} - \chi_c}{R_{inc} + R_{bg} + R_{soil}}. \tag{5}$$

Following the parameterizations for R_{inc}, R_{bg}, and R_{soil} described by Pleim (2006) and Cooter et al. (2010), it is apparent that R_{soil} is the limiting resistance. While the dynamics of the in-canopy atmospheric resistances will drive the variability of the soil flux on a short timescale (Bash et al.,
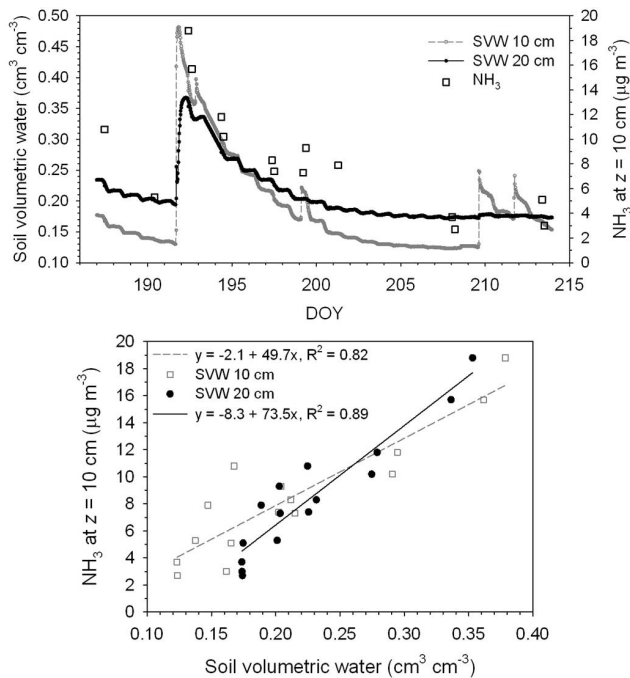
Fig. 10. Time series of soil volumetric water during in-canopy measurement period along with NH_3 air concentration at $z = 10\,cm$ above the soil surface (top graph); correlation between NH_3 concentration at $z = 10\,cm$ and soil volumetric water at 10 and 20 cm depth (bottom graph). Soil volumetric water data represent 30-min averages, and air concentrations represent 2-h integrated samples.

2010), we find that the concentration of NH_3 measured just above the soil surface ($z = 0.1\,m$) was strongly linked to soil moisture on a timescale of days to weeks. Figure 10 shows a time series of soil volumetric water content at 10 and 20 cm depth along with the concentration of NH_3 at 10 cm above the soil surface over the 26-day period during which in-canopy concentrations were measured. The surface air concentration follows the pattern of soil moisture quite closely, exhibiting high correlation with moisture at both 10 and 20 cm depths (Fig. 10). Ammonia concentrations just above the soil are higher immediately after the rainfall on DOY 191 relative to the samples preceding the rain event and decrease over time as the soil dries.

The correlation between the concentration of NH_3 just above the soil surface and soil moisture likely reflects a combination of chemical and physical processes. The NH_3 flux from the soil surface is linked to soil moisture via resistance to NH_3 diffusion through the soil profile, which decreases non-linearly with increasing soil moisture. As described by Sakaguchi and Zeng (2009), the soil resistance is a function of the ratio of the length of the dry soil layer, through which a gas must diffuse to the atmosphere, to the gas diffusion coefficient. As the soil dries, the length of the diffusion path increases, thereby increasing the resistance to the diffusive flux. This effect may be reflected in Fig. 10 as the soil dries

following the heavy rainfall on DOY 191. On a timescale of days, the supply of NH_3 in the lower canopy, and therefore available for transport to the atmosphere, was apparently limited by the soil resistance as regulated by soil water content. It is possible, however, that the relationship shown in Fig. 10 represents the dynamics of both the soil resistance and NH_4^+ pool. As indicated in Fig. 6, Γ_{soil} decreases during the period shown in Fig. 10, though only two Γ_{soil} samples are available. The temporal pattern of the NH_3 air concentrations shown in Fig. 10 may therefore partly reflect a coincident decrease in the soil emission potential. Urea hydrolysis would also exhibit a positive relationship with soil moisture. If significant concentrations of urea persisted this late into the growing season, the decrease in Γ_{soil} may partly reflect the relationship between urea hydrolysis and soil moisture content.

3.6.3 Foliage

The analysis presented by Bash et al. (2010) established that the foliage was a large sink for NH_3 emitted from the soil during the day. Here we extend that analysis by partitioning the bulk foliage flux into cuticular and stomatal components, using measured stomatal resistances for H_2O and NH_3 compensation points derived from measured apoplast chemistry. The cuticular and stomatal fluxes are constrained by the total (net) canopy-scale and ground fluxes estimated from the analytical source/sink model of Bash et al. (2010). Following the resistance framework employed within CMAQ (Bash et al., 2012), the total (net) flux (F_t) above the canopy is equivalent to

$$F_t = \frac{(\chi_c - \chi_a)}{R_a + 0.5 \cdot R_{inc}} = F_g + F_s + F_w, \tag{6}$$

where χ_c is the canopy compensation point ($\mu g\,NH_3\,m^{-2}$), χ_a the air concentration measured at the top of the canopy ($\mu g\,NH_3\,m^{-2}$), F_g the ground flux ($ng\,m^{-2}\,s^{-1}$) estimated via the analytical source/sink model, F_s the stomatal flux ($ng\,m^{-2}\,s^{-1}$) and F_w the cuticular flux ($ng\,m^{-2}\,s^{-1}$). In this analysis, F_t is also estimated via the analytical source/sink model and F_s is calculated as

$$F_s = \frac{(\chi_s - \chi_c)}{R_b + R_{st}}, \tag{7}$$

where χ_s is the stomatal compensation point estimated from measured apoplast H^+ and NH_4^+ concentrations during period B (Table 1) using Eq. (2).

Equations for the aerodynamic (R_a), boundary layer (R_b) and in-canopy (R_{inc}) resistances were summarized by Pleim (2006). The NH_3 concentration profile in vegetation canopies is not constant, and NH_3 can be exchanged with foliage along this gradient (Bash et al., 2010). In order to reconcile this with a resistance model framework, R_{inc} is split in Eq. (6) such that half of the resistance is applied between the soil and the canopy compensation point (χ_c) and the other half

from the canopy to the atmosphere above. This was done to account for NH$_3$ emitted from the soil that is not subjected to the entire in-canopy aerodynamic resistance before exposure to foliage surfaces. After calculating χ_c from Eq. (6) and F_s from Eq. (7), F_w is calculated as

$$F_w = F_t - F_s - F_g. \qquad (8)$$

Ignoring one measurement period conducted entirely at night, the remaining ($N = 14$) in-canopy periods yielded mean (median) stomatal and cuticular fluxes of $-32(-10)$ and $-94(-84)$ ng NH$_3$ m^{-2} s^{-1}, respectively. The ratio of median and mean fluxes, respectively, suggests that stomatal uptake accounts for 12–34 % of the total foliage flux during the day, the balance being attributed to the cuticular flux. Dominance of the cuticular pathway is partly due to the relatively large minimum stomatal resistance of NH$_3$, which was 154 ± 17 s m^{-1} at a PAR level of 1800 μmol m^{-2} s^{-1} and 30 °C as derived from measured leaf-level H$_2$O resistances adjusted for differences in molecular diffusivity. The flux budget derived by Bash et al. (2010) in combination with the analysis presented here is summarized in Fig. 11.

Given the relatively high emission potential measured in the leaf surface water, apparent dominance of the cuticular flux during the day suggests that the chemistry of the wet cuticle is not necessarily indicative of the resistance characteristics of the dry cuticle. This is somewhat supported by the results in Table 3, which indicate lower net-canopy emissions (i.e., greater recapture by the leaf cuticle surface) when the canopy is dry. The in-canopy measurements summarized by Bash et al. (2010) are limited to a single measurement (DOY 199, 05:30–08:20) during which the canopy was wet for the entire observation period. The source/sink modeling results of Bash et al. (2010) indicate that the canopy recaptured 43 % of the NH$_3$ emitted from the soil during this observation period, compared to 78 % recapture derived from median fluxes during the six observation periods in which the canopy was completely dry. During the DOY 199 morning measurement period, a canopy concentration (χ_c) of 7.9 μg m^{-3} is estimated from the source/sink resistance modeling described above, compared to a leaf droplet compensation point (χ_d) of 6.3 μg m^{-3} derived from leaf droplet chemistry measured on the morning of DOY 200, indicating that the surface droplets were capable of NH$_3$ uptake. Though the canopy was wet, partitioning of the foliage flux as described above indicated that F_w (-8 ng m^{-2} s^{-1}) was half of F_s (-16 ng m^{-2} s^{-1}). This single observation is generally consistent with the pattern of larger cuticular resistances under wet conditions reflected in Table 3.

Regarding the leaf surface water, the most prominent feature of the diurnal profile of the net canopy-scale flux (Fig. 5) during period B is a large emission peak in the morning, coincident with drying of the canopy and rapid mixing of the surface layer. Based on destructive sampling and weighing of wet leaves on two occasions between sunrise and 10:00, we estimated the water content of the middle and upper
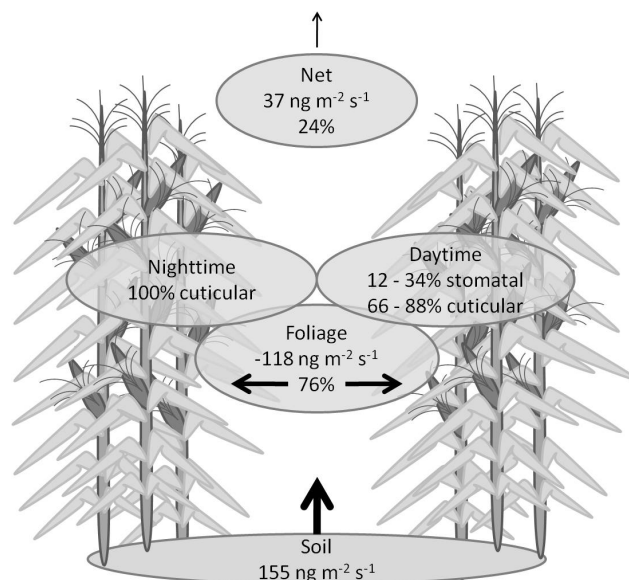
Fig. 11. Summary of average soil, foliage and net canopy fluxes calculated by Bash et al. (2010) using an analytical source/sink model with the foliage flux further partitioned into estimated stomatal and cuticular components. Note that results represent conditions near peak LAI.

canopy to be 25–35 g H$_2$O m^{-2}, which typically dried completely by 09:30. Based on the maximum measured concentration of NH$_4^+$ (2990 μg L^{-1}) in dew and guttation and a LAI of 3.0 m^2 m^{-2}, the maximum possible flux associated with complete drying of the canopy between sunrise and 09:30 is 17.6 ng NH$_3$ m^{-2} s^{-1}, compared to mean and median fluxes between 07:00 and 10:00, which encompasses the period during which the flux typically increases to its morning peak, of 137 and 43 ng NH$_3$ m^{-2} s^{-1}. While a much larger contribution to the net flux may be observed if the majority of the NH$_3$ volatilization were confined to the late stages of the canopy drying, our results suggest that the morning emission peak cannot be entirely explained by desorption associated with the drying of the canopy. It is more likely that the morning peak in NH$_3$ air concentrations and fluxes above the canopy results from a combination of canopy drying, drying of the moisture that accumulates on the soil surface at night, and venting of NH$_3$ that accumulates within the canopy and below the lowest NH$_3$ sampling inlet under stable nighttime conditions. This hypothesis is supported by the temporal pattern of changes in in-canopy concentration profiles during 6 sequential periods from 01:00 to 14:30, which showed a reduction in the in-canopy concentrations post-sunrise consistent with the above-canopy late morning peak in concentration (Bash et al., 2010).

Overall, the comparison of the emission potentials of soil, leaf surface water (dew/guttation) and foliage suggests that any emission from the canopy does not originate from the foliage. This is consistent with an intensive examination of

the various NH_4^+ pools in an agricultural grassland canopy, which also showed emission potentials of the soil and decomposing plant parts to exceed those of live leaves (Sutton et al., 2009).

4   Conclusions

Results from this study illustrate the magnitude and temporal characteristics of NH_3 emissions from a fertilized corn canopy. The dynamics of the flux during the first month after fertilization were influenced by both the characteristics of the fertilizer, which contained a urease inhibitor, and the temperature and moisture content of the soil. While total losses of NH_3 were consistent with emission factors for UAN solutions with urease inhibition, the temporal distribution of the post-fertilization flux, which primarily occurred in two distinct emission pulses, may not be well simulated by current soil process models.

In-canopy source/sink modeling showed that the foliage has a large capacity to recapture emissions from the soil during the day once the canopy has fully developed. In light of this result, it is important to remember that fertilizer loss studies, which typically rely on chamber-based soil flux measurements, may not necessarily represent expected crop-level net emissions from the complete soil/vegetation system. Re-adsorption of soil NH_3 emissions by the overlying vegetation may also be considered by growers as a crop characteristic that could be managed to help optimize nitrogen efficiency and reduce N volatilization losses from fertilizer. Future work should quantitatively address this question for other crop types, planting densities, and fertilizer characteristics within the context of yield optimization through management of crop N requirements by growth stage. Our estimates of 76 % canopy recapture of soil emissions represent conditions expected of a fully developed canopy after the soil flux has diminished over a period of several weeks following fertilization. As total adsorption by the overlying canopy is a function of vegetation density, recapture rates for the entire growing season would be much lower. This should be quantitatively examined in future studies. Finally, our results underscore the importance of modeling NH_3 air–surface exchange using a bi-directional, compensation point approach in regional air quality models, which accounts for the effects of soil/canopy interactions on net fluxes from fertilized soils.

From a process standpoint, our results indicate that soil moisture positively influences soil NH_3 emissions throughout the growing season. Future experimental work should seek to reduce uncertainties in soil resistance parameterizations for NH_3, which will require measurements that decouple the relationships between soil moisture and the dynamics of the soil NH_4^+ pool versus the resistance to NH_3 diffusion through the soil profile. Secondly, we deduce that cuticular uptake was reduced when the canopy was wet due to leaching of base cations from the leaf and solubilization of alkaline

particles on the leaf surface. In systems where a lack of turbulent mixing generally minimizes fluxes at night, this feature of the cuticular exchange process may not be important with respect to total fluxes. However, cuticular uptake was estimated to be larger when the canopy was dry and dominated the total foliage exchange during the day. This unique relationship between canopy wetness and cuticular resistance points to the remaining uncertainty in the current understanding of the dynamics of leaf surface chemistry as the canopy dries. Development of experimental approaches to better understand this process for the purpose of improving cuticular resistance parameterizations represents a challenging but important step forward.

Supplementary material related to this article is available online at: http://www.biogeosciences.net/10/981/2013/bg-10-981-2013-supplement.pdf.

References

Bash, J. O., Walker, J. T., Jones, M., Katul, G., Nemitz, E., and Robarge, W.: Estimation of in-canopy ammonia sources and sinks in a fertilized Zea mays field, Environ. Sci. Technol., 44, 1683–1689, 2010.

Bash, J. O., Cooter, E. J., Dennis, R. L., Walker, J. T., and Pleim, J. E.: Evaluation of a regional air-quality model with bi-directional NH_3 exchange coupled to an agro-ecosystem model, Biogeosciences Discuss., 9, 11375–11401, doi:10.5194/bgd-9-11375-2012, 2012.

Burkhardt, J. and Eiden, R.: The ion concentration of dew condensed on Norway spruce (*Picea abies* (L.) Karst.) and Scots pine (*Pinus sylvestris* L.) needles, Trees, 4, 22–26, 1990.

Burkhardt, J., Flechard, C. R., Gresens, F., Mattsson, M., Jongejan, P. A. C., Erisman, J. W., Weidinger, T., Meszaros, R., Nemitz, E., and Sutton, M. A.: Modelling the dynamic chemical interactions

of atmospheric ammonia with leaf surface wetness in a managed grassland canopy, Biogeosciences, 6, 67–84, doi:10.5194/bg-6-67-2009, 2009.

Chadwick, D., Misselbrook, T., Gilhespy, S., Williams, J., Bhogal, A., Sagoo, L., Nicholson, F., Webb, J., Anthony, S., and Chambers, B.: Ammonia emissions and crop N use efficiency, Component report for Defra project NT2605/WP1b, 2005.

Chow, J. C., Chen, L.-W. A., Watson, J. G., Lowenthal, D., Magliano, K., Turkiewicz, K., and Lehrman, D.: PM$_{2.5}$ chemical composition and spatiotemporal variability during the California Regional PM$_{10}$/PM$_{2.5}$ Air Quality Study (CRPAQS), J. Geophys. Res., 111, D10S04, doi:10.1029/2005JD006457, 2006.

Cooter, E., Bash, J. O., Walker, J. T., Jones, M., and Robarge, W.: Estimation of NH$_3$ bi-directional flux from managed agricultural soils, Atmos. Environ., 44, 2067–2166, 2010.

Dawson, G. A.: Atmospheric ammonia from undisturbed land, J. Geophys. Res., 82, 3125–3133, 1977.

Denmead, O. T., Freney, J. R., and Dunin, F. X.: Gas exchange between plant canopies and the atmosphere: case-studies for ammonia, Atmos. Environ., 42, 3394–3406, 2008.

Dennis, R. L., Mathur, R., Pleim, J., and Walker, J. T.: Fate of ammonia emissions at the local to regional scale as simulated by the Community Multiscale Air Quality model, Atmos. Pollut. Res., 1, 207–214, 2010.

Edgerton, E. S., Hartsell, B. E., Saylor, R. D., Jansen, J. J., Hansen, D. A., and Hidy, G. M.: The Southeastern Aerosol Research and Characterization Study: Part 2, Filter-based measurements of fine and coarse particulate matter mass and composition, J. Air Waste Manage., 55, 1527–1542, 2005.

European Centre for Ecotoxicology and Toxicology of Chemicals (ECETOC): Ammonia emissions to air in Western Europe, Technical Report 62, Brussels, Belgium, 1994.

Farquhar, G. D., Firth, P. M., Wetselaar, R., and Weir, B.: On the gaseous exchange of ammonia between leaves and the environment: determination of the ammonia compensation point, Plant Physiol., 66, 710–714, 1980.

Flechard, C., Fowler, D., Sutton, M. A., and Cape, J. N.: A dynamic chemical model of bi-directional ammonia exchange between semi-natural vegetation and the atmosphere, Q. J. Roy. Meteor. Soc., 125, 2611–2641, 1999.

Gilliland, A. B., Dennis, R. L., Roselle, S. J., and Pierce, T. E.: Seasonal NH$_3$ emission estimates for the Eastern United States based on ammonium wet concentrations and an inverse modeling method, J. Geophys. Res., 108, 4477, doi:10.1029/2002JD003063, 2003.

Gioacchini, P., Nastri, A., Marzadori, C., Giovannini, C., Antisari, L. V., and Gessa, C.: Influence of urease and nitrification inhibitors on N losses from soils fertilized with urea, Biol. Fert. Soils, 36, 129–135, 2002.

Goebes, M. D., Strader, R., and Davidson, C.: An ammonia emission inventory for fertilizer application in the United States, Atmos. Environ., 37, 2539–2550, 2003.

Harper, L. A. and Sharpe, R. R.: Nitrogen dynamics in irrigated corn: Soil nitrogen and atmospheric ammonia transport, Agron. J., 87, 669–675, 1995.

Harper, L. A., Denmead, O. T., and Sharpe, R. R.: Identifying sources and sinks of scalars in a corn canopy with inverse Lagrangian dispersion analysis II. Ammonia, Agric. Forest Meteorol., 104, 75–83, 2000.

Hsieh, C., Katul, G., and Chi, T.: An approximate analytical model for footprint estimation of scalar fluxes in thermally stratified atmospheric flows, Adv. Water Resour., 23, 765–772, 2000.

Husted, S. and Schjoerring, J. K.: Apoplast pH and ammonium concentration in leaves of *Brassica napus* L., Plant Physiol., 109, 1453–1460, 1995.

Hutchinson, T. C., Adams, C. M., and Gaher, B. A.: Neutralization of acidic raindrops on leaves of agricultural crop and boreal forest species, Water Air Soil Poll., 31, 475–484, 1986.

Malm, W. C., Sisler, J. F., Huffman, D., Eldred, R. A., and Cahill, T. S.: Spatial and seasonal trends in particle concentration and optical extinction in the United States, J. Geophys. Res., 99, 1347–1370, 1994.

Massad, R.-S., Nemitz, E., and Sutton, M. A.: Review and parameterisation of bi-directional ammonia exchange between vegetation and the atmosphere, Atmos. Chem. Phys., 10, 10359–10386, doi:10.5194/acp-10-10359-2010, 2010.

Mathur, R. and Dennis, R. L.: Seasonal and annual modeling of reduced nitrogen compounds over the Eastern United States: emissions, ambient levels, and deposition amounts, J. Geophys. Res., 108, 1–19, 2003.

Mecklenburg, R. A., Tukey Jr., H. B., and Morgan, J. V.: A mechanism for the leaching of calcium from foliage, Plant Physiol., 41, 610–613, 1966.

Meyers, T. P., Hall, M. E., Lindberg, S. E., and Kim, K.: Use of the modified Bowen-ratio technique to measure fluxes of trace gases, Atmos. Environ., 30, 3321–3329, 1996.

Moldrup, P., Oleson, T., Yamaguchi, T., Schjonning, P., and Rolston, D. E.: Modeling diffusion and reaction in soils: IX. The Buckingham-Burdine-Campbell equation for gas diffusivity in undisturbed soil, Soil Sci., 164, 542–555, 1999.

National Atmospheric Deposition Program/National Trends Network, http://nadp.sws.uiuc.edu/, last access: March 2012.

Nemitz, E., Sutton, M. A., Gut, A., San José, R., Husted, S., and Schjørring, J. K.: Sources and sinks of ammonia within an oilseed rape canopy, Agric. Forest Meteorol., 105, 385–404, 2000.

Nemitz, E., Milford, C., and Sutton, M. A.: A two-layer canopy compensation point model for describing bi-directional biosphere-atmosphere exchange of ammonia, Q. J. Roy. Meteor. Soc., 127, 815–833, 2001.

Nihlgard, B.: The ammonium hypothesis – an additional explanation to the forest dieback in Europe, Ambio, 14, 2–8, 1985.

Paerl, H. W. and Whitall, D. R.: Anthropogenically derived atmospheric nitrogen deposition, marine eutrophication and harmful algal bloom expansion: is there a link?, Ambio, 28, 307–311, 1999.

Pleim, J. E: A simple, efficient solution of flux–profile relationships in the atmospheric surface layer, J. Appl. Meteorol. Clim., 45, 341–347, 2006.

Rawluk, C. D. L., Grant, C. A., and Racz, G. J: Ammonia volatilization from soils fertilized with urea and varying rates of urease inhibitor NBPT, Can. J. Soil Sci., 8, 239–246, 2001.

Robarge, W. P., Walker, J. T., McCulloch, R. B., and Murray, G.: Atmospheric concentrations of ammonia and ammonium at an agricultural site in the southeast United States, Atmos. Environ., 36, 1661–1674, 2002.

Roelle, P. A. and Aneja, V. P.: Characterization of ammonia emissions from soils in the upper coastal plain, North Carolina, At-

mos. Environ., 36, 1087–1097, 2002.

Sakaguchi, K. and Zeng, X.: Effects of soil wetness, plant litter, and under-canopy atmospheric stability on ground evaporation in the Community Land Model (CLM3.5), J. Geophys. Res. Atmos., 114, D01107, doi:10.1029/2008JD010834, 2009.

Sutton, M. A., Burkhardt, J. K., Guerin, D., Nemitz, E., and Fowler, D: Development of resistance models to describe measurements of bi-directional ammonia surface-atmosphere exchange, Atmos. Environ., 32, 473–480, 1998.

Sutton, M. A., Nemitz, E., Milford, C., Campbell, C., Erisman, J. W., Hensen, A., Cellier, P., David, M., Loubet, B., Personne, E., Schjoerring, J. K., Mattsson, M., Dorsey, J. R., Gallagher, M. W., Horvath, L., Weidinger, T., Meszaros, R., Dämmgen, U., Neftel, A., Herrmann, B., Lehman, B. E., Flechard, C., and Burkhardt, J.: Dynamics of ammonia exchange with cut grassland: synthesis of results and conclusions of the GRAMINAE Integrated Experiment, Biogeosciences, 6, 2907–2934, doi:10.5194/bg-6-2907-2009, 2009.

US EPA: Compendium Method IO 4.2: Determination of Reactive Acidic and Basic Gases and Strong Acidity of Fine-Particles ($< 2.5\,\mu m$). EPA/625/R-96010a; US EPA: Cincinnati, OH, 1997.

US EPA: National Emissions Inventory, http://www.epa.gov/ttn/chief/net/2002inventory.html#inventorydata, (last access: March 2012), 2005.

Vlek, P. L. G. and Carter, M. C.: The effect of soil environment and fertilizer modifications on the rate of urea hydrolysis, Soil Sci., 136, 56–63, 1983.

Walker, J. T., Robarge, W. P., Wu., Y., and Meyers, T.: Measurement of bi-directional ammonia fluxes over soybean using the modified Bowen-ratio technique, Agr. Forest Meteorol., 138, 54–68, 2006.

Watson, C. J., Miller, H., Poland, P., Kilpatrick, D. J., Allen, M. D. B., Garrett, M. K., and Christianson, C. B.: Soil properties and the ability of the urease inhibitor N-(n-butyl) thiophosphoric triamide (nBTPT) to reduce ammonia volatilization from surface-applied urea, Soil Biol. Biochem., 26, 1165–1171, 1994.

Watson, C. J., Akhonzada, N. A., Hamilton, J. T. G., and Matthews, D. I.: Rate and mode of application of the urease inhibitor N-(n-butyl) thiophosphoric triamide on ammonia volatilization from surface-applied urea, Soil Use Manage., 24, 246–253, 2008.

Wolff, V., Trebs, I., Ammann, C., and Meixner, F. X.: Aerodynamic gradient measurements of the NH_3–HNO_3–NH_4NO_3 triad using a wet chemical instrument: an analysis of precision requirements and flux errors, Atmos. Meas. Tech., 3, 187–208, doi:10.5194/amt-3-187-2010, 2010.

Wyers, G. P., Otjes, R. P., and Slanina, J.: A continuous-flow denuder for the measurement of ambient concentrations and surface exchange of ammonia, Atmos. Environ., 27A, 2085–2090, 1993.